Tooling and procedures for hybrid integration of lasers by flip-chip technology

Colin J Mitchell
Optoelectronics Research Centre
University of Southampton
Southampton, UK
c.j.mitchell@soton.ac.uk

Ke Li
Optoelectronics Research Centre
University of Southampton
Southampton, UK
kl@ecs.soton.ac.uk

Ralph Schachler
Finetech GmbH & Co
Berlin, Germany
ralph.schachler@finetech.de

Ali Khokhar
Optoelectronics Research Centre
University of Southampton
Southampton, UK
a.z.khokhar@soton.ac.uk

Xia Chen
Optoelectronics Research Centre
University of Southampton
Southampton, UK
xia.chen@soton.au.uk

Stevan Stanković
Optoelectronics Research Centre
University of Southampton
Southampton, UK
ORCID: 0000-0001-6154-3138

Xiangjun Wang
Optoelectronics Research Centre
University of Southampton
Southampton, UK
xiangjun.wang@soton.ac.uk

Neil P Sessions
Optoelectronics Research Centre
University of Southampton
Southampton, UK
nps@orc.soton.ac.uk

Katarzyna M Grabska
Optoelectronics Research Centre
University of Southampton
Southampton, UK
kmg1d19@soton.ac.uk

David J Thomson
Optoelectronics Research Centre
University of Southampton
Southampton, UK
d.thomson@soton.ac.uk

Christoph Daedlow
Finetech GmbH & Co
Berlin, Germany
christoph.daedlow@finetech.de

Graham T Reed
Optoelectronics Research Centre
University of Southampton
Southampton, UK
g.reed@soton.ac.uk

James S Wilkinson
Optoelectronics Research Centre
University of Southampton
Southampton, UK
ORCID: 0000-0003-4712-1697

***Abstract*—A method of achieving hybrid integration of laser bars on a silicon platform, using chip-flip bonding, is presented. A support structure etched into the substrate is used to provide vertical alignment to the plane utilizing a gimballed placement laser tool. In-plane accuracy is provided by bonder tolerances, with facet-to-facet alignment enabled by high magnification optics and the dimensions of the laser bar. Chip design features have increased allowed tolerances during fabrication of the support structure giving a route to higher yield in manufacture.**

Keywords—laser, integration, hybrid, flip-chip, passive alignment, silicon photonics

I. Introduction

Light sources for silicon photonics remain a major focus of investigation internationally, from small scale demonstrators through to production level systems. Integrated, or on-chip, sources in particular are an enabling technology to access the huge potential of silicon photonics as a key disruptive technology. The issue arises because the performance of lasers based upon silicon itself [1] is not currently suitable for Photonic Integrated Circuit (PIC) requirements, although improvements have been made in recent years [2]. This is largely due to the indirect bandgap of silicon, unlike the compound semiconductors used in commercial lasers.

Approaches to realize integration of on-chip sources include wafer bonding, token/transfer printing and growth of efficient gain material on silicon substrates such as the Silicon-On-Insulator (SOI) platform routinely used in silicon photonics. Lasers may be fabricated directly on the PIC from this deposited or bonded material, easing some alignment issues and incorporating evanescent coupling. Each of these techniques has advantages and also technical difficulties. A further approach is to use conventional pre-packaged III-V lasers. This can be implemented in a number of ways. For example, lasers can be mounted in a stand-a-lone module (complete with lens, isolator and mirror) for bonding and coupling to a grating [3, 4], or an integrated structure with a lens that can be fabricated in the III-V gain material [5]. A more conventional technique is to bond a fabricated laser directly on to a PIC with the emission either grating-coupled

Fig. 1. Finetech Fineplacer® Lambda

This work was supported by the UK EPSRC Programme Grant, Silicon Photonics for Future Systems EP/L00044X/1

or butt-coupled into a waveguide. The latter approach is discussed here, coupling to the facet of a silicon optical waveguide.

II. Hybrid Integration: Pre-fabricated Laser Bonding

Using III-V lasers with silicon photonic circuits enables optimal materials to be used for each component: the light source and the photonic circuit. Coupling these as a back-end process allows existing dedicated production facilities to fabricate each component separately. Testing of these components occurs independently in this case, potentially increasing final yield. The laser and PIC can subsequently be integrated at an isolated location to reduce any contamination to the main fabrication facilities such as between group IV and III-V elements (dopants to each other), as well as the associated process issues that arise, contrasting the needs of each independent material system.

A hybrid approach such as this, using pre-fabricated lasers, requires very small placement tolerances in six degrees of freedom. Misalignment typically needs to be less than 0.5 µm in all direction for the case of a 1.55 µm laser and SOI circuit [6]. This is usually achieved by active alignment of the laser, where the laser is operational during bonding and alignment, allowing coupling between laser and circuit to be measured on the PIC. In this way alignment can be optimised before fixing the laser in place. Such a system can be automated [7] and used for either the lasers modules described earlier or direct PIC integration. This requires electrical and/or optical contact to the chip as well as electrical contact to the laser. Achieving similar high precision with passive alignment using flip-chip bonding would lead to a reduction of manufacturing complexity and the associated time and cost.

The integration of multiple lasers simultaneously using a single laser bar (multiple lasers fabricated on a single chip) is shown not only to be possible, but when incorporated effectively it is positively used to enable greater placement accuracy in the work presented here.

III. Flip-Chip Bonding Technique

Laser chips are positioned face-down on top of a face-up PIC by means of a flip chip bonder (see Fig. 1). Alignment is made with the placement arm in the vertical position (Fig. 2b), this is achieved optically. The images of the two components are superimposed upon each other via a beamsplitter imaging system as shown in Fig. 2. The image shown through the beamsplitter will be the relative location of the components after coming into physical contact. Larger versions of the tool replace the beam splitter with two separate cameras.

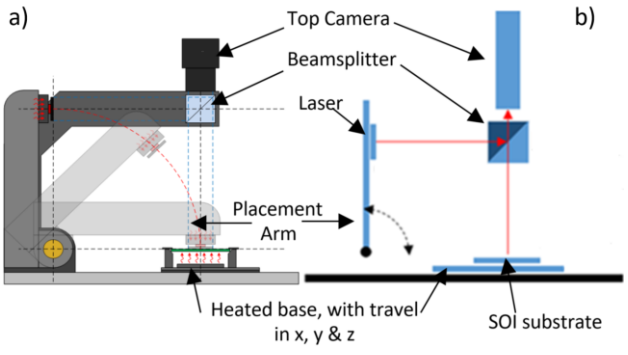

Fig. 2. a) Principle of operation, and b) schematic

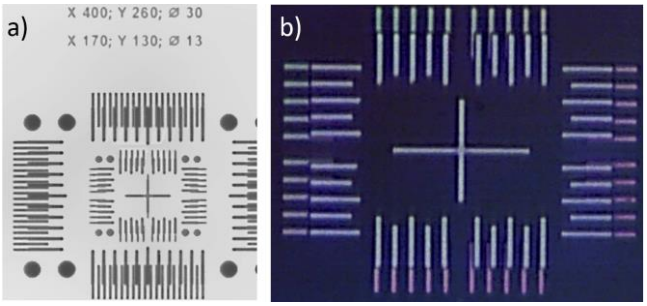

Fig. 3. a) Calibration glasses aligned, and b) at high magnification showing minor misalignment

Calibration of the beam splitter determines the placement accuracy. This is achieved by using two transparent quartz slides each with markings to allow a Vernier scale measurement when in contact with each other. The slides are aligned using the beamsplitter and placed upon each other as if bonding. The Vernier scales, visible through the quartz, then gives a direct measurement of alignment (see Fig. 3b). Adjustment to the beam splitter can then be made iteratively (align, place, measure, adjust) until optimal alignment is achieved. Depending upon the tool and type of alignment optics utilized, accuracies down to 0.3 µm with three-sigma conformity (>99.7%) have been demonstrated as a standard specification by Finetech in an automated version of the tool, demonstrating the ability to scale this laser integration technique for automated manufacturing.

The manual alignment tools, as used here, rely upon the resolution of the Vernier scales described above. The limit of the Vernier offset for manual alignment of the calibration optics (Fig. 3) is 0.5 µm per Vernier mark, this is derived from the capabilities for accurate visualization by the camera, limiting resolution of the accuracy measurement. This limit to alignment measurement does not necessarily define the limit of achievable alignment however, purely the measurable value. The specific vale for actual misalignment can be better than 0.5 µm, especially with high magnification optics. To qualify this, consider a misalignment of between 0.5 µm intervals as in Fig 3b, but less than 0.5µm.

IV. Design Implications

The improving accuracy of flip-chip bonders now enables acceptable tolerances in the plane of alignment of the component, i.e. x and y placement (see Fig. 4), for the application as described above. However, the vertical placement, z, is not easily controlled to the tolerances required. In this case, the required alignment of the laser mode is to a waveguide with a thickness of 220 nm or 400 nm, depending upon the silicon photonics SOI platforms being

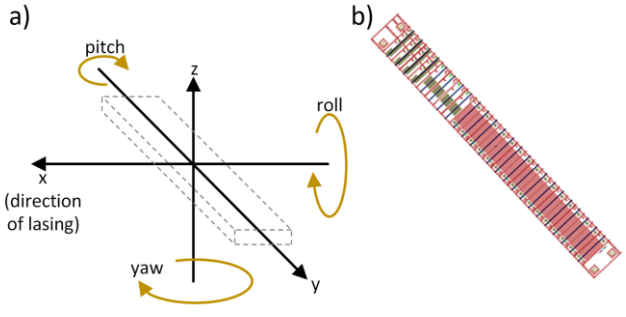

Fig. 4. a) Six degrees of freedom, b) laser bar

used. This requires a z-alignment (height – see Fig 4a) tolerance to be better than the thickness of the waveguide to achieve reasonable coupling of the overlapping and dispersive modes from the waveguide and laser facets.

Conventional flip-chip bonding for electronic integrated circuits usually requires the chip to be held in position at a fixed height (controlled by the bonder) in contact with melted solder balls that are cooled. As the solder cools it solidifies and defines the vertical position, as well as forming contacts and fixing the bar in position.

To control the height position to achieve the required tolerance (smaller than the waveguide thickness), an enhanced method is required. Here, we utilize separate support structures on the SOI (see Fig. 5) to control the vertical location of the laser bar relative to the SOI [6, 8, 9]. Hence, the vertical alignment that controls the coupling of the laser and waveguide modes is defined as part of the fabrication process.

A. Support Structure

There are two vertical dimensions to consider to maximise coupling (Z_1 and Z_2 in Fig. 5): the position of the centre of each of the two modes (laser and waveguide) relative to the point of contact between the laser bar and the SOI. The issue is how accurately can the point of contact on each component, relative to the modes, be controlled or defined. This controls the alignment of the modes and hence the mode overlap.

The support structures are fabricated from the SOI substrate in this case, eliminating any error from the deposition of other materials in addition to any etch. The vertical position of the support, relative to the position of the waveguide and its mode on the SOI, is controlled entirely by etch tolerance and this can be controlled within the order of 10 nm, dependent upon tooling. On the laser component, the position of the mode within the structure can be modelled and measured, relative to the surface of the laser, for a particular design and is constant.

In order to achieve the best possible alignment, we specify that the locations (on the laser) of contact to the SOI support structures remain unprocessed, i.e. no metal contacts, etch or isolation dielectric. The distance from the centre of the laser mode to the surface of the laser (point of contact) is then fixed by laser design.

This method eliminates processing variations for the lasers affecting vertical alignment, as well as flip-chip tooling height placement variations. The only variable is the support

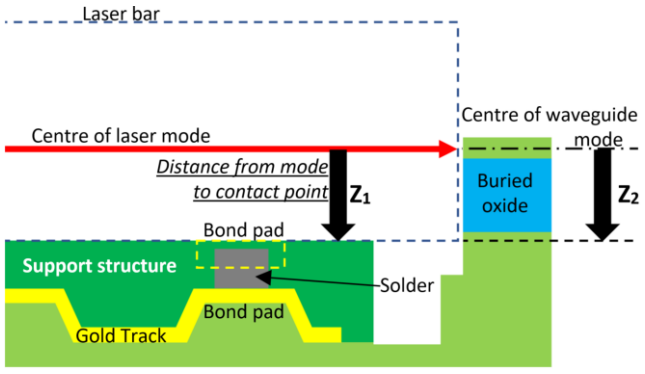

Fig. 5. Support structure and laser schematic (side view)

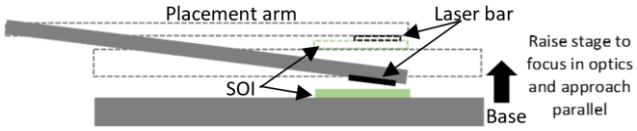

Fig.6. Placement arm and pitch alignmentwith vertical position of the base (short edge)

structure etch depth, which can be controlled with very high accuracy (±10 nm), exceeding the required tolerance.

B. Laser Bar and Degrees of Freedom

The basic method outlined above requires some refinement when considering a real system. All degrees of freedom require accuracy: x-y-z placement in addition to angular alignment of pitch, roll, and yaw (Fig. 4a). The angular alignment is particularly important when considering larger laser dies, for example laser bars, where angular misalignment will not just affect the direction of the beam, but also the x-y-z alignment. Shown in Fig. 4b is an example of the laser bars used for this work in order to demonstrate the relative dimensions, with the test structures to the left and the active lasers to the right. The laser bar dimensions used in this work were 14.5 x 1.5 mm, hosting sixteen DFB lasers (operating at 1529 nm), and various test structures. Each individual laser had a separate absorber section to allow direct measurement of output power from the rear facet. This resulted in a device with two top surface contact pads for each laser at either edge and a common contact on the reverse of the laser bar.

An advantage of using a larger sample, such as a laser bar, is that yaw alignment can be improved. This is achieved by performing alignment at either end of the laser bar, in the same manner that fiducial marks are placed at either extreme of a conventional lithography mask. This is enabled by the bonding tool having the provision for the alignment optics to move in the y-direction as defined in Fig. 4 along the edge of the laser bar, whilst the beamsplitter does not move, thus maintaining its calibrated position.

C. Roll and Pitch

The final generalized consideration for alignment is that this method will only work if the laser bar can be placed parallel to, and in contact with, the SOI support structure surfaces, i.e. within roll and pitch tolerances.

A schematic of the placement arm and base is shown in Fig. 6. Considering the height of the base and the SOI together, the height will give a potential source of pitch error that can be adjusted. However, if both surfaces are in focus they are equidistant from the beam splitter and as such, by

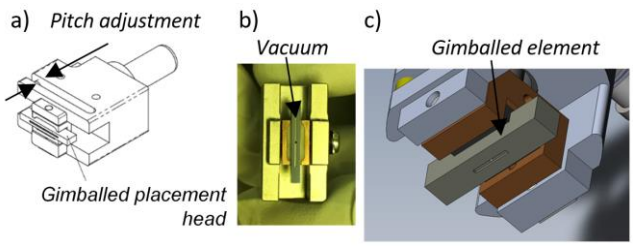

Fig. 7. Single-axis gimbal laser placement tool, a) the single axis gimbal shown within the placement tool, b) an image of the tool showing vacuum contact, c) schematic of the tool (rotating element in grey)

design, the components surfaces will be very close to parallel. Some small error will still exist without further consideration of alignment and is discussed below whilst addressing the issue of roll adjustment.

To fully compensate for any roll error in placement from the rigid flip-chip mechanism a single-axis gimballed placement head (see Fig. 7) was used. This enabled the laser bar to be placed absolutely flat (see Fig. 8) in the y-direction along the long dimension of the laser bar. This eradicates roll misalignment completely for a die with no physical defects on the components and an intact support structure. The placement head also has adjustment for fine alignment of pitch. Pitch is adjusted by a screw on the placement head and inspected by the side camera (shown in Fig. 1) on maximum magnification. This does not eradicate pitch error completely, but does reduce it to acceptable levels (as will be shown later). Visual inspection through the side camera on high magnification clearly shows a sub-micrometre error across the width, allowing accurate alignment. An alternative is to use a two-axis gimbal, but in the case of a long laser bar the short side's gimbal does not work effectively in some cases, depending upon the relative dimensions and therefore rotational forces acting upon the chip.

A principle of design of the bonding tool is to reduce moving components, and therefore sources of potential placement error. In the case of a gimballed tool the placement accuracy requires assessment due to the mechanical components. Testing of the single-axis gimbal tool typically demonstrates no measureable loss in accuracy in the y-direction (i.e. 0.5 µm or less), and a slightly increased misalignment in the x-direction (facet-to-facet) giving between 0.5 µm and 1.0 µm, measured using the Vernier scale calibration quartz (Fig 3b).

D. Alignment Considerations

The final position of the laser on the SOI is visually determined through the beam splitter as described above. The mechanism for doing that is facet-to-facet alignment of the lasers and waveguides, not by using fiducials. This is to eradicate any error from the position of the fiducial relative to the cleaved laser facet.

Whilst using a facet-to-facet direct alignment, in order to make the alignment as accurate as possible, the highest possible magnification optics should be used with the beam splitter. The optics used in this application facilitated a total system optical resolution of 0.7 µm (see Fig. 9), i.e. the resolution of optics, camera and monitor combined. Automated pattern recognition systems can perform sub-pixeling of identical images allowing much more precise alignment than the actual image resolution. This is also typically the case with manual machines where human operators naturally perform the same function on an image, enabling alignment of the centres of blurry lines for example.

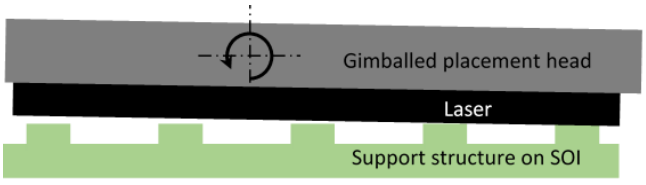

Fig. 8. Parallel alignment along long edge of laser bar using a gimbal mechanism

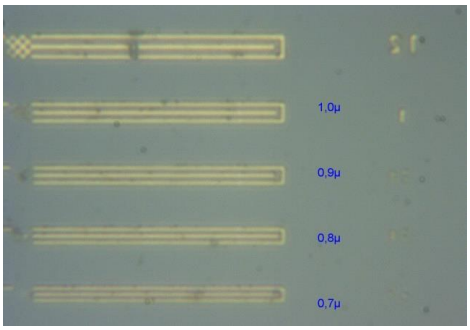

Fig. 9. Optical resolution down to 0.7 µm with Finetech A7+ optics

A demonstration of the facet-to-facet alignment through the beam splitter is shown in Fig. 10, where a 2 µm wide laser is aligned to a 10 µm wide waveguide. The final accuracy of placement is then defined by the calibration of the beamsplitter as described earlier.

An important consideration when relying upon the magnification of the optics to perform the alignment is that the optics should be centred at, or very near to, the point of alignment (i.e. the facets as in Fig. 10) and not the centre of the chip. In the latter case magnification may have to be reduced to include the point of alignment in the image, as well as the centre point. This would reduce accuracy. Adjustment of the point of focus on the chip can be achieved in two ways. Firstly, by moving the mounting position of the chip (either relative to the placement arm or by moving the placement arm itself). Or secondly by moving the optics, without moving the beamsplitter (in the same way as described earlier when sweeping along the long edge of the chip). In either case, the former was used for this work, the position will usually require adjustment in two dimensions (x and y) to align to the first and last laser facet on the laser bar whilst retaining full magnification.

E. Electrical Contacts

Electrical contacts between the laser bar and the SOI were required between respective bond pads (see Fig. 10 for the overlay image), namely between the bond pads on the SOI and the laser bar's active lasing section and absorber monitor for each of the sixteen devices on each laser bar. Due to the presence of the support structure, and by design of a suitable flow channel for excess solder, the volume of solder between connecting pads on the laser and SOI does not determine height alignment. Excess solder is pushed clear in the liquid phase until the two components are in contact at the supports. This allows for a greater margin of error when depositing the solder compared to alignment by surface tension for example, where the dimensions of the solder are critical as well as the wetting properties of the bond pads and their precise dimensions and edge definition [8]. Excess solder flow was

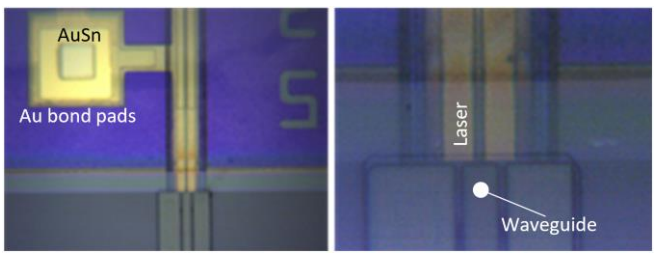

Fig.10. Alignment, viewed through the beamsplitter prior to contact and bonding, of a 2 µm wide laser to a 10 µm waveguide.

controlled by using trenches that surround the contact pads on the SOI (see Fig. 5 and Fig. 11a). Excess solder will 'squirt' out in one direction should the surface tension fail, and not spread evenly. This required the development of angled etches, over which to run the contacting tracks, provided by either wet etch (TMAH) or latterly dry etch in ICP-RIE.

Contacts to a III-V compound semiconductor lasers are usually provided by a final gold layer, due to the properties of the materials at the metal-semiconductor interface. Gold was used on the laser bars used here, and therefore chosen for the corresponding contacts on the SOI.

A gold-tin alloy with composition close to the gold-rich eutectic point (melting at 280ºC), was used as the solder between the gold metal contacts on the laser and SOI. This provided a low thermal budget, mechanical strength and excellent Ohmic properties between the gold pads on either component [10].

The main consideration for the solder deposition and formation becomes the thickness of the solder. The thickness only has to exceed the gap between the gold bond pads when the chip and laser bar are placed together (see Fig. 5), and by standard thickness to provide good electrical characteristics. Once the components are in contact, under a controlled force, the solder is melted by heating from the bonder's base (via the SOI). The excess solder in the molten form is pushed away and the device is cooled with the components held in place, resulting in the relative positions being frozen in place with the separation defined by the support structure only.

With the reduction of tolerance required for the solder definition in this method, deposition and formation can be easily controlled within the limits required. The solder was e-beam evaporated and patterned on the SOI substrate using a standard lift-off technique. In Fig. 10 both bond pads (laser and SOI) as well as the smaller square of gold-tin solder can be seen overlaid in the beamsplitter image during final alignment.

F. Methodology and Fabrication Considerations

The design allows for tolerances between features to be as large as possible to allow issues such as step coverage and definition to be more easily controlled with thick lithography photoresists, making the process as robust as possible.

The bottom of the buried oxide was used as an etch stop, combining dry etch (ICP-RIE for vertical sidewalls) and wet etch, to control etch depths of the supports to high accuracy (± 10 nm) without in-situ monitoring.

Waveguides were written by e-beam lithography, with a subsequent facet etch across the waveguide to give best possible resolution of the facet, but could equally be formed by alternative lithography processes. A range of angles for the waveguide facet were included in the design to reduce reflections/feedback to the lasers. Output grating couplers were fabricated at the opposite end of the waveguide in order to couple light out for measurement. The gratings were designed to be long (200 µm) in order to couple the majority of the light out along the length of the grating, but with low efficiency to minimise reflections back through the waveguide to the laser. This restricted the reflections back to the laser to predominantly those from the waveguide facet, allowing assessment of the facet reflections isolated from other factors. The collected power from the gratings for a standard fibre diameter was therefore reduced as not all the light could be coupled to a single fibre core. The final design after fabrication (before bonding) is shown in Fig. 11a.

A statistical consideration affecting yield comes from the size of the support structures themselves. The structures needed to be large enough in area to support the laser and be mechanically robust, but as small as possible to decrease the probability of defects misaligning the sample in the z-direction or pitch/roll.

Implications of the theoretical and actual topography of the lasers, such as bowing and edge defects were considered, and also accounted for in the design. The co-dependence of the components' fabrication tolerances are clear, and indeed critical to success.

The issues outlined above demonstrate the theoretical and practical method that was employed. The design of the support structures, contact metal and surrounding features all determine the probabilities of success. This is not just in addition to, but holistically alongside, the tooling capabilities and the stringent fabrication tolerances for the laser structure. Process and assembly tolerances have been considered, eased and eradicated where possible by design. The cumulative effect of small variations is the key concept.

V. PERFORMANCE

Laser bars were characterized before bonding to enable comparisons to be made to the final integrated device. This included electrical and optical measurements, with correlation

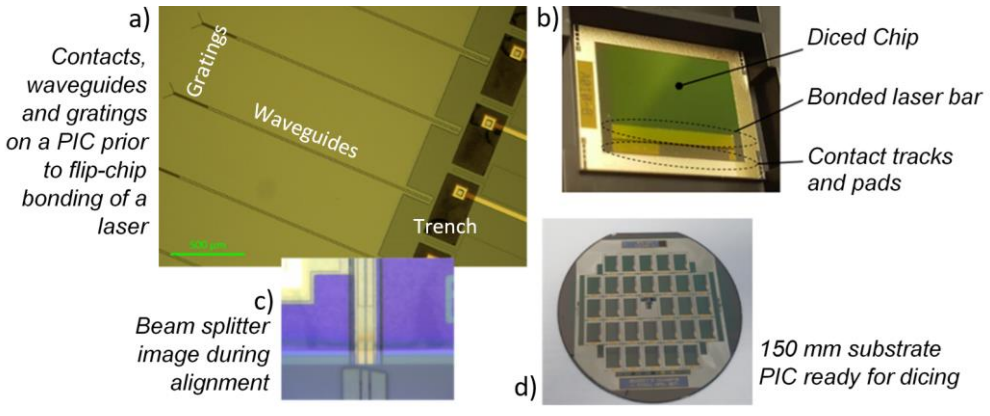

Fig. 11. SOI circuit and chip, a) Fabricated SOI substrate showing waveguides, gratings, solder trench and contacts, b) a laser bonded to SOi, c) angled waveguide facet during alignment, d) fabricated 6" (150 mm) SOI substrate

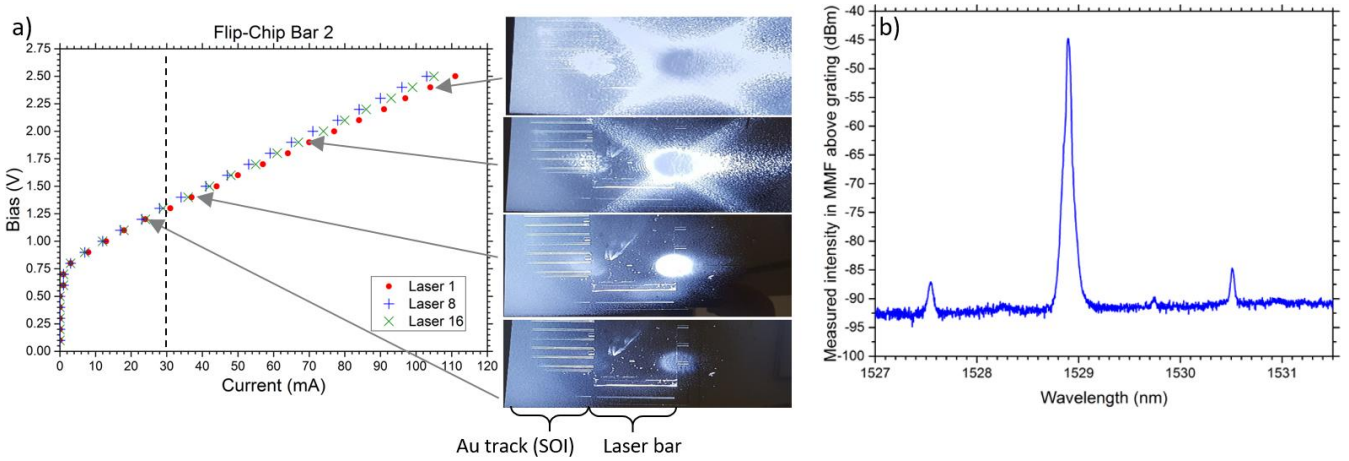

Fig. 12. Optical output from lasers, a) with current-voltage for three lasers and IR camera from above, b) collected spectrum

between absorber section current (at fixed reverse bias) and the measured optical power output of the laser.

Once bonded (see Fig. 11b), the electrical contacts to the laser bars demonstrated uniform current-voltage characteristics across each of the sixteen individual lasers (as well as absorbers) on each laser bar and between the four laser bars mounted. This gave a yield for electrical contacts of 100%. A comparison of typical laser current-voltage characteristics is shown in Fig. 12a.

Importantly the yield of the electrical contacts demonstrates the placement tolerances that were achieved, considering the excess thickness of the solder was of the order of 300 nm and the locations of the bond pads. Specifically, this demonstrates the tolerances achieved in z-direction (height), pitch and roll across the length of the laser bar in order to achieve contact between the pads from the solder. This rationale considers the location at either edge of the laser bar of the absorber and laser contacts, i.e. uniform contacts at both edges of the laser bar and along the length of the laser bar (14.5 mm by 1.5 mm) with a maximum error of no more than 300 nm, and probably much smaller considering the uniform data across multiple samples.

In addition, the relationship between measured current at the absorber section and laser drive currents remained identical before and after bonding. This indicates no loss of power output from the laser resulting from integration of the device, either from electrical bonding or reflection/coupling to the waveguides.

Optical output of the laser was demonstrated using an infrared camera above a bonded sample. A series of such images is shown in Fig. 12a for increasing drive current, from below the expected threshold drive current of 30 mA, to above. The onset of lasing is clearly evident. All measurements were CW (up to 220 mA, with 120 mA shown) and uncooled.

Optical output from the SOI waveguides was collected through a multimode optical fibre aligned to the grating output couplers on the SOI. The fibres were connected to an optical spectrum analyser, and also a power meter, to acquire data. Emission was confirmed to be from the waveguide mode as the angle of the collecting fibre to the grating output providing maximum coupled power, corresponded to the that of the fundamental guided mode at the grating and by sweeping data points across gratings (y-direction). A typical spectrum is given in Fig. 12b, and closely matches the spectrum measured before bonding, maintaining side-mode suppression (over 40 dBm in the example below).

Work is underway to efficiently collect all the waveguide-coupled power and estimate the waveguide input coupling efficiency. Characterisation to determine coupling efficiency versus SOI waveguide facet angle has also begun. High-resolution spectral measurements using the self-heterodyne technique will also be made to determine any changes in wavelength, linewidth or spectral purity due to facet reflections into the cavity. These measurements have already been made for the standalone laser.

VI. Summary

It is desirable for the purposes of yield and ease of manufacture to make alignment processes for integration of lasers and laser bars with silicon photonic circuits as passive as possible, whilst maintaining fabrication tolerances that are as large as possible. Using this philosophy III-V DFB laser bars, providing simultaneous bonding of multiple lasers, have been successfully flip chip bonded to an SOI silicon photonics platform using a Finetech FINEPLACER® Lambda bonding tool. This utilized novel support structures and contacts in conjunction with specific tooling requirements and processing considerations. The combination of good design of the host SOI chip (including support structures, contact, waveguide circuit design etc.) and high precision in-plane placement from the bonding tool allowed passive alignment and coupling to silicon waveguides.

Important design considerations, tooling issues, and fabrication issues for the SOI circuit have been presented, demonstrating the potential for on-chip integration across a wide range of wavelengths and laser designs. This method has now been successfully transferred to other material systems, including germanium-on-silicon waveguides for laser wavelengths in the mid-infrared.

Acknowledgment

D. J. Thomson acknowledges funding from the Royal Society for his University Research Fellowship.

All data supporting this study are openly available from the University of Southampton repository at https://doi.org/10.5258/SOTON/D1419.

REFERENCES

[1] D. Liang, J. E. Bowers, “Recent progress in lasers on silicon”, Nature Photon 4, pp 511–517, July 2010

[2] Dong-Chen Wang, Chi Zhang, Pan Zeng, Wen-Jie Zhou, Lei Ma, Hao-Tian Wang, Zhi-Quan Zhou, Fei Hu, Shu-Yu Zhang, Ming Lu, Xiang Wu, “An all-silicon laser based on silicon nanocrystals with high optical gains”, Science Bulletin, vol 63, issue 2, pp 75-77, January 2018

[3] De Dobbelaere, P., Armijo, G., Balardeta, J., Chase, B., Chi, Y., et al. “Silicon-photonics-based optical transceivers for high-speed interconnect applications”, Proc. of SPIE vol. 9775 977503-2, March 2016

[4] M. Mack, M. Peterson, S. Gloeckner, A. Narasimha, R. Koumans, and P. De Dobbelaere,“Method and system for a light source assembly supporting direct coupling to an integratedcircuit,” (2012). US Patent 8,168,939.

[5] K. Adachi, T. Suzuki, K. Nakahara, S. Tanaka, A. Nakanishi, K. Naoe, “A facet-free 1.3-μm surface-emitting DFB laser for alow-cost optical module”, IEICE Electronics Express, vol.13, no.21, pp 1–6, October 2016

[6] A. Moscoso-Mártir, F. Merget, J. Mueller, J. Hauck, S. Romero-García, B. Shen, F. Lelarge, R. Brenot, A. Garreau, E. Mentovich, A. Sandomirsky, A. Badihi, D. E. Rasmussen, R. Setter, J. Witzens, “Hybrid silicon photonics flip-chip laser integration with vertical self-alignment”, 2017 Conference on Lasers and Electro-Optics Pacific Rim (CLEO-PR), Singapore, 2017, pp. 1-4

[7] G. Böttger, D. Weber, F. Scholz, H. Schröder, M. Schneider-Ramelow, et al., “Fully automated hybrid diode laser assembly using high precision active alignment”, Proc. SPIE 9730, Components and Packaging for Laser Systems II, 97300E, 22 April 2016

[8] Y. Martin, S. Kamlapurkar, N. Marchack, J. Nah and T. Barwicz, "Novel Solder Pads for Self-Aligned Flip-Chip Assembly," 2019 IEEE 69th Electronic Components and Technology Conference (ECTC), Las Vegas, NV, USA, 2019, pp. 528-534

[9] Y. Martin, J.S. Orcutt, C. Xiong, L. Schares, T. Barwicz, M. Glodde, S. Kamlapurkar, E.J. Zhang, W.M.J. Green, V. Dolores-Calzadilla, A. Sigmund, M. Moehrle, "Flip-Chip III-V-to-Silicon Photonics Interfaces for Optical Sensor," 2019 IEEE 69th Electronic Components and Technology Conference (ECTC), Las Vegas, NV, USA, 2019, pp. 1060-1066

[10] J.W. Ronnie Teo, F.L. Ng , L.S. Kip Goi, Y.F. Sun, Z.F. Wang, X.Q. Shi, J. Wei, G.Y. Li, “Microstructure of eutectic 80Au/20Sn solder joint in laser diode package” Microelectronic Engineering, vol 85, issue 3, pp 512-517, March 2008